The Incorporation of Organ Uptake into Dynamic SPECT (dSPECT) Image Reconstruction

T. Farncombe[†], A. Celler[‡] *Member, IEEE*, C. Bever[†], D. Noll [¶], J. Maeght[¶], R. Harrop[‡] *Member, IEEE*
[†]Department of Physics, University of British Columbia, Vancouver, B.C., Canada
[‡]Division of Nuclear Medicine, Vancouver Hospital and Health Sciences Centre, Vancouver, B.C., Canada
[¶]Mathématiques pour l'Industrie et la Physique, Université Paul Sabatier, Toulouse, France.

Abstract

Dynamic SPECT (dSPECT) is an image reconstruction method capable of determining three dimensional regional estimates of physiological kinetic rates while still maintaining the simple acquisition protocol of a single, slow camera rotation. Through the use of inequality constraints in a least squares optimization routine, we are able to determine both the rate of tracer uptake and subsequent tracer washout over the acquisition time of the SPECT scan.

Simulations modelling different camera acquisition geometries and with variable dual exponential kinetic parameters and model complexity (eg, statistical noise, object attenuation) were performed. It was found that kinetic parameters were accurate to within 50% of the true values for the case of fast uptake and slow washout for a single head acquisition and improved to within 95% when acquired with a triple head camera. Experimental phantom tests corraborated these results and are shown to have an accuracy of about 90%. A preliminary patient study of renal dynamics has also been performed and compared with conventional planar dynamic imaging. Results from this study indicate that the dSPECT reconstruction method is able to determine kinetic information with accuracy comparable to that of conventional planar dynamic imaging methods while providing additional three dimensional time behaviour information.

I. Introduction

In SPECT, the determination of the kinetic parameters associated with a regional (ie, three dimensional) activity change due to underlying metabolic processes is a problem that has been investigated using multiple head, fast rotation acquisition methods, [1] [2], or with the slow rotation constrained least squares (CLS) approach with appropriate decreasing activity constraints, [3] [4]. The latter method has advantages as it uses a conventional SPECT acquisition procedure, but has the necessary condition that the activity within all pixels must decrease over the data collection period. In practice, this condition often is not true for all pixels since, as a consequence of activity washout in some regions, other regions must increase in activity. In these circumstances, some pixels will be reconstructed erroneously with this method. Additionally, in many clinical circumstances (eg., renal glomerular filtration rate), the rate of activity uptake into an organ is a useful measure of the organ's functional ability. For these reasons, it would be beneficial to include the possibility of an increasing activity into the CLS dSPECT approach in order to obtain three dimensional dynamic information and to take advantage of the simplified acquisition protocol offered by the dSPECT method. In this work, an extension to the CLS method of dSPECT reconstruction is presented in an effort to reconstruct both organ uptake and washout using a slow SPECT camera rotation.

II. The CLS Approach

The dSPECT reconstruction process is aimed at reconstructing an unknown object activity distribution as a series of images where each image corresponds to the spatial distribution of activity at a particular time. In the case of a decreasing activity distribution, this can be described as,

$$\text{minimize } f(x) = \left\{ \sum_{j,k} \sigma_{jk}^{-2} \left(\sum_i C_{ijk} x_{ik} - d_{jk} \right)^2 \right\} \quad (1)$$

$$\text{subject to } x_{i1} \geq x_{i2} \geq \ldots \geq x_{in} \geq 0 \quad (2)$$

where σ_{jk}^{-2} is a weighting factor determined from the variance of the projection bin contents d_{jk}; C_{ijk} is a geometrical weighting factor that may incorporate attenuation correction and collimator blurring; and x_{ik} represents the reconstructed activity in the *i*th pixel at the time of the *k*th projection.

Following data reconstruction, a series of images is obtained where each image corresponds to the activity distribution within the object at the time of each projection measurement. Analysis of this data can then be carried out either by fitting this data to the appropriate compartmental model in order to determine kinetic parameters or by drawing three dimensional regions of interest and plotting the number of counts within each region against time in a 3D time activity curve (3D-TAC). This TA curve can then further be fit to an appropriate pharmacokinetic model in order to determine regional kinetic parameters.

It should be pointed out that the constraint (2) represents only the case for activity washout from the object. A modification can easily be applied to allow for an increasing activity distribution over the imaging time by simply replacing the $\geq$ symbols with the $\leq$ symbol. As well, the positivity constraint must also be maintained in the reconstructed object activities and thus, for an object with increasing activity, the inequality constraint becomes,

$$0 \leq x_{i1} \leq x_{i2} \leq \ldots \leq x_{in} \quad (3)$$

A. Activity Uptake

In many situations, radiopharmaceutical washout is not the only process that is relevent clinically but rather the rate of pharmaceutical uptake into an organ can often be useful in the diagnosis of disease. In situations such as this, it would be expected that the rate of organ uptake is more rapid than that corresponding to tracer washout. As well, this process would generally be faster than the imaging time of the SPECT acquisition. The activity distribution within an organ exhibiting such behaviour would increase initially up to a time t_p, followed by a slow decline corresponding to the tracer washout.

Such a change in activity can be dealt with in the CLS dSPECT method by combining inequalities (2) and (3) in order to reconstruct an increasing activity up to time t_p, and then subsequent tracer washout after this point. Thus, the modified constraint for each i-th pixel can be written as,

$$0 \leq x_{i1} \leq \ldots \leq x_{ip-1} \leq x_{ip} \geq x_{ip+1} \geq \ldots \geq x_{in} \geq 0 \quad (4)$$

It should be pointed out that each pixel may have a different point t_p that must be known in order that the constraint (4) be applied correctly. In clinical data, this point can never be known *a priori*, and for such cases, the following technique is used to determine it.

B. Determination of Peak Pixel Activity Time

Consider the combined increasing and decreasing activity time activity curve for a single pixel as shown below in Figure 1a). For this pixel, the position of peak activity occurs at projection number 15 of 64, therefore, the modified inequality constraint should be:

$$0 \leq x_{i1} \leq \ldots \leq x_{i14} \leq x_{i15} \geq x_{i16} \geq \ldots \geq x_{i64} \geq 0 \quad (5)$$

Though this position is not known prior to the image reconstruction process, it can be determined by performing two initial reconstructions on the same dynamic data; one assuming all pixels to decrease in activity over the scan time, and the other one assuming all pixels to increase over time. The TA curves for these reconstructions are shown in Figure 1b). Notice that when reconstructed using the decreasing only constraint, the time activity curve reconstructs correctly after projection 30, but remains flat in the region 1-29. Similarly the increasing only reconstruction yields time frames 1-7 reconstructing correctly as increasing, but with the times 8-64 depicted as static. If the correct portions of these two reconstructions are combined (ie, projections 1-7 and 30-64), a flat region extends over projections 8-29, thus indicating that the true peak activity is situated somewhere in this interval. Therefore, as a first guess, we simply use the point midway on this plateau (projection 18) as the point t_p in the CLS reconstruction algorithm.

Since the estimated peak position is not known exactly, a further modification is made to the inequality constraint (4) to

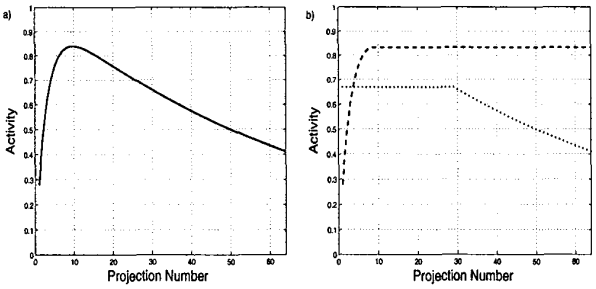

Figure 1: a) The true time activity curve (TAC) for a dynamic increasing/decreasing simulation. b) The reconstructed TAC for the simulation assuming only increasing, and only decreasing activity.

allow some flexibility in the peak position. This is done by modifiying the inequality (4) such that $2x_{ip} \geq x_{ip-1} + x_{ip+1}$. With this modification, the peak position can now occur at any of the positions x_{ip-1}, x_{ip} or x_{ip+1}, and is free to move to any of these positions during the reconstruction process.

III. Simulations and Experiments

A. Computer Simulations

As an initial test of the modified constraint dSPECT method, we performed a variety of computer simulations modelling various acquisition protocols and dynamic behaviours. The first dynamic simulation consisted of an annulus divided into four equally sized regions (237 pixels each). True images were simulated as 64x64 pixel matrices with an outer diameter of 40 pixels, and an inner diameter of 20 pixels (Figure 2). The activity present within each region of the annulus was described by a dual exponential function,(6),

$$A(t) = A_0(-e^{-\lambda_1 t} + e^{-\lambda_2 t}) \quad (6)$$

representing both increasing and decreasing portions. Functional parameters are summarized in Table 1. Additional randomly distributed Poisson noise was added to the projection measurements in proportion to the number of counts collected in each camera bin ($\approx$ 18 % at peak activity) .

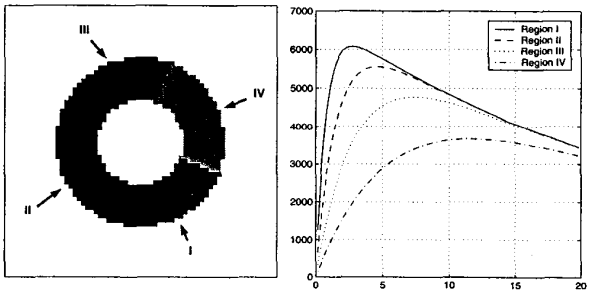

Figure 2: a) The dynamic annulus simulation phantom shown at t = 5 min. b) The time activity curves for each of the four dynamic regions.

Additionally, we have performed a variety of computer simulations based upon a simplified model of fatty acid metabolism within the myocardium [5]. Our model consisted

Region	Peak (min)	A_0 (counts)	$T_{\frac{1}{2},\lambda_1}$ (min)	$T_{\frac{1}{2},\lambda_2}$ (min)
I	2.8	6854	0.5	20.0
II	4.7	6854	1.0	20.0
III	7.5	6854	2.0	20.0
IV	11.9	6854	4.0	20.0

Table 1: Dual exponential function parameters used in dynamic simulations involving the annulus phantom.

of a heart object positioned within a non-uniform attenuating thorax with a warm constant background (see Figure 3). The heart object is further divided into two sections with each section displaying different initial activity concentrations and undergoing different dual exponential behaviour (equation (6) as summarized in Table 2. Initial object activity consisted of a total of 0.1 mCi in the myocardium which corresponds to a 7% uptake of a 20 mCi injection distributed over 15 slices in the heart. Again, randomly generated Poisson noise corresponding to these activity levels for each projection measurement was added to the data in a manner similar to the annulus phantom.

Region	Peak (min)	A_0 (counts)	$T_{\frac{1}{2},\lambda_1}$ (min)	$T_{\frac{1}{2},\lambda_2}$ (min)
I	3.4	2332	1.0	8.0
II	5.9	4615	2.0	10.0
III	0.0	7354	∞	∞

Table 2: Function parameters used in dynamic heart simulations.

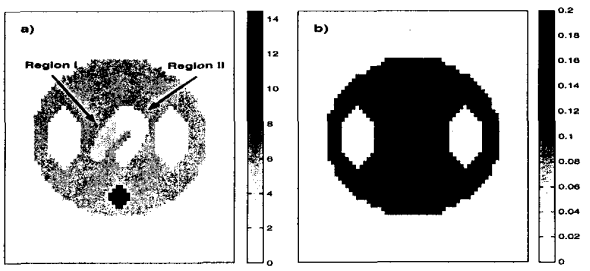

Figure 3: a) The dynamic heart thorax phantom shown at t = 10 s. b)The nonuniform thorax attenuation map used in simulations.

In both simulations, projection data was acquired for a single transverse slice assuming perfect, parallel hole collimation. Data was simulated with single, dual, and triple head gamma cameras, over acquisition times of 20 minutes. In all cases, data was collected with identical angular sampling intervals of 2.8°, corresponding to 64 projection measurements per head over 180°. Acquisition protocols for each simulation are summarized in Table 3.

B. *Phantom and Patient Experiments*

In order to further validate our CLS method, we have performed experiments using our dynamic heart phantom [6] in the absence of additional attenuating medium. Dynamic data containing uptake and washout was acquired by injecting a bolus of activity into a small container, followed by constant

Acquisition Geometry	Rotation Angle	Camera Bins	Stops (per head)	Time (min)
1 head	180°	64	64	20 min
2 heads, 90°	180°	64	64	20 min
3 heads, 120°	180°	64	64	20 min

Table 3: Acquisition parameters used in computer simulations.

dilution with pure water. The effect of this procedure is a quick increase in radiotracer activity in the bottle, followed by a monoexponential washout with rate determined by the flow of the incoming water.

In these experiments, a total of eight different dynamic containers were imaged (five bottles in experiment 1 and three bottles in experiment 2). Projection measurements were acquired using a Siemens Ecam dual head camera system with the heads in the 90° configuration and with a camera rotation of 90° per head. Each container was imaged independently so that the true dynamic behaviour of each bottle could be determined directly from the projection measurements (possible only in the absence of appreciable attenuation). Time activity curve data was fit with a three parameter dual exponential function, eqn. (6) with the true parametric values summarized in Table 4. To create multiple object data sets, projection data for the individual containers were then summed together to create two separate, multiple bottle, dynamic SPECT data sets.

Experiment 1

Region	A_0 (counts)	$T_{\frac{1}{2},\lambda_1}$ (min)	$T_{\frac{1}{2},\lambda_2}$ (min)
I	25512	0.02	2.0
II	21786	0.02	3.8
III	18007	0.05	37.8
IV	22436	0.04	6.7
V	19330	0.05	10.2

Experiment 2

Region	A_0 (counts)	$T_{\frac{1}{2},\lambda_1}$ (min)	$T_{\frac{1}{2},\lambda_2}$ (min)
I	24224	0.15	1.8
II	20484	0.28	3.8
III	26050	0.63	5.4

Table 4: True parametric values used in the dynamic heart-in-thorax experiments.

As an initial application of the CLS dSPECT method to clinical data, we have performed a study of the renal dynamics of Tc-99m MAG3. 10 mCi of Tc-99m labelled MAG3 were injected into a healthy volunteer and SPECT imaging was performed using a dual head Siemens Ecam camera with the heads in the 90° configuration and involving a rotation of 90° per head. Projection data was collected into 128x128 matrices with 64 stops per head over a total acquisition time of 12 minutes. A simultaneous transmission scan using the Profile transmission apparatus was performed in order to

obtain a patient specific attenuation map. A few hours prior to the SPECT data acquisition, a dynamic planar renogram was acquired using 1 mCi of MAG3 in order to compare with the dSPECT reconstructions.

IV. Methods of Analysis

In order to quantitatively assess the accuracy of dSPECT reconstructions, different figures of merit have been utilized depending on the *a priori* knowledge of the object. When the true object activity is known (as in the case for computer simulations), two different accuracy assessment methods have been used: i) a direct comparison between true dynamic rate constants and those obtained by fitting the appropriate time dependent function to the reconstructed data for each dynamic region, and ii) an assessment of the relative standard deviation, ε, between the true and reconstructed activities for a given region, R, where,

$$\varepsilon_R = \sum_k W_{k'} \frac{\sigma_k}{\mu_k} \tag{7}$$

where σ_k is the standard deviation between the true and reconstructed pixel activies at each k-th time frame, μ_k is the true activity at each time frame, and $W_{k'}$ represents a weighting factor equal to,

$$W_{k'} = \frac{\mu_{k'}}{\sum_k \mu_k} \tag{8}$$

Parametric fits to reconstructed time activity curves were found by minimizing the χ^2 between the estimated parametric values, and the reconstructed time activity curves for each region. An additional test of accuracy was made in the determination of the peak activity position within each region. For this measurement, a standard deviation measurement was made between the true peak position for each pixel and the position determined by the dSPECT method. Values for this quantity are referred to in terms of the time of peak activity.

In order to determine the true dynamic rates when experimental phantom data was used, each object was imaged separately with no object attenuation. For each projection, all camera pixels were summed together in order to create a time activity curve for the entire region. The resultant TA curves were then fit to the appropriate three parameter, biexponential increasing/decreasing function, (equation (6)), in order to determine the true dynamic rate constants.

Following dSPECT image reconstruction of the combined object data sets, three dimensional regions of interest were drawn on each container and a time activity curve obtained. Again, the data from these TA curves were fit with three parameter biexponential functions and the results compared with the TA curve parameter fits acquired from the projection data of each individual object.

The patient data is the most difficult to quantitively evaluate due to the lack of knowledge of the true dynamic behaviour. Therefore at this stage, we have chosen to evaluate this data by comparison to planar dynamic imaging on a qualitative basis only.

V. Results

A. Computer Simulations

Results of the reconstruction accuracy for simulation studies are summarized in Tables 5a and 5b. Typical reconstruction images are depicted in Figure 4.

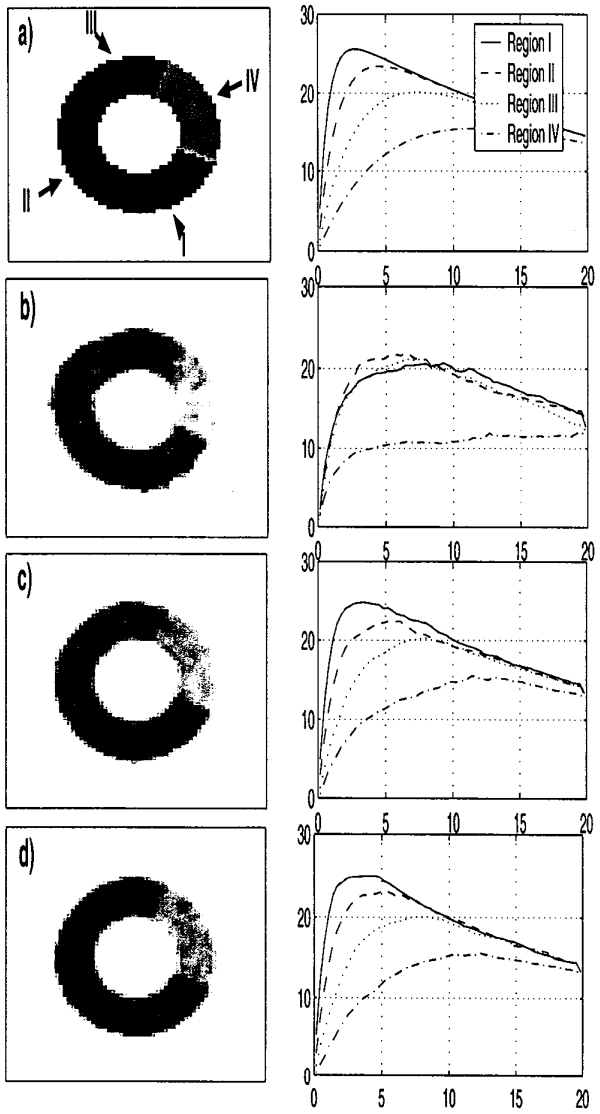

Figure 4: a)The true annulus phantom at t = 5 min, and the time activity curves for each region divided by the number of pixels per region. Results of the dSPECT reconstruction are shown for b) single head acquisition, c) dual head camera acquisition, and d) triple head camera acquisition.

Based upon values of the cumulative relative error and the quality of reconstructed images, it appears that the CLS method is able to reconstruct the true time activity curves of each pixel to reasonable accuracy, even in the case of a single

Acquisition	Region Error			
	I	II	III	IV
Single head	0.37	0.43	0.51	0.38
Dual head	0.33	0.35	0.42	0.29
Triple head	0.30	0.35	0.41	0.28

Table 5a: Weighted relative standard deviation measurements for each dynamic region of the annulus phantom acquired with the three different acquisition geometries.

Region	Peak Time	A_0 (counts)	$T_{\frac{1}{2},\lambda_1}$ (min)	$T_{\frac{1}{2},\lambda_2}$ (min)
Single head				
I	9.3 ± 6.8	5469	1.1	30.8
II	7.8 ± 3.7	6415	1.0	17.5
III	8.9 ± 2.3	5957	1.2	23.6
IV	11.3 ± 2.2	2604	0.99	57.9
Dual head				
I	5.7 ± 3.5	6694	0.6	20.0
II	6.8 ± 2.8	6288	0.9	21.0
III	8.3 ± 1.8	6742	2.0	20.0
IV	10.9 ± 2.6	3906	2.5	78.0
Triple head				
I	5.5 ± 3.4	6725	0.5	19.6
II	6.7 ± 2.9	6649	1.0	20.6
III	8.7 ± 2.4	6982	2.1	18.5
IV	10.9 ± 2.6	7062	4.2	18.9

Table 5b: Parametric fits for the CLS reconstructed annulus simulation phantom (cf. Table 1).

detector head. As expected, reconstructions utilizing additional data obtained with multiple head cameras result in lower error values, thus indicating more accurate reconstruction. However, the increase in accuracy obtained using a triple head camera appears only marginally better than that obtained with a dual head geometry.

It should be recognized that in some of the time activity curve fits, a significant difference can be seen between the true dynamic parameters and the reconstructed TA curve parameters (eg. Dual head, Region IV). This effect is not as significant as it may appear at first glance and is related to the inherent difficulty in fitting multiple exponential functions to data. It is possible when fitting multiple exponential functions that widely different parametric values will fit the same data equally well.

Simulations of the dynamic heart model indicate similar results to the annulus (Figure 5 and Tables 6a and 6b), again with the triple head camera yielding the lowest error values. Once again however, reconstructions using the triple head camera performs only marginally better than the dual head camera undergoing a 180° rotation per head. In every simulation, it is clear that single head rotations are not practical with the current implementation of the CLS method, and that for more faithful reconstructions at least two camera heads are necessary.

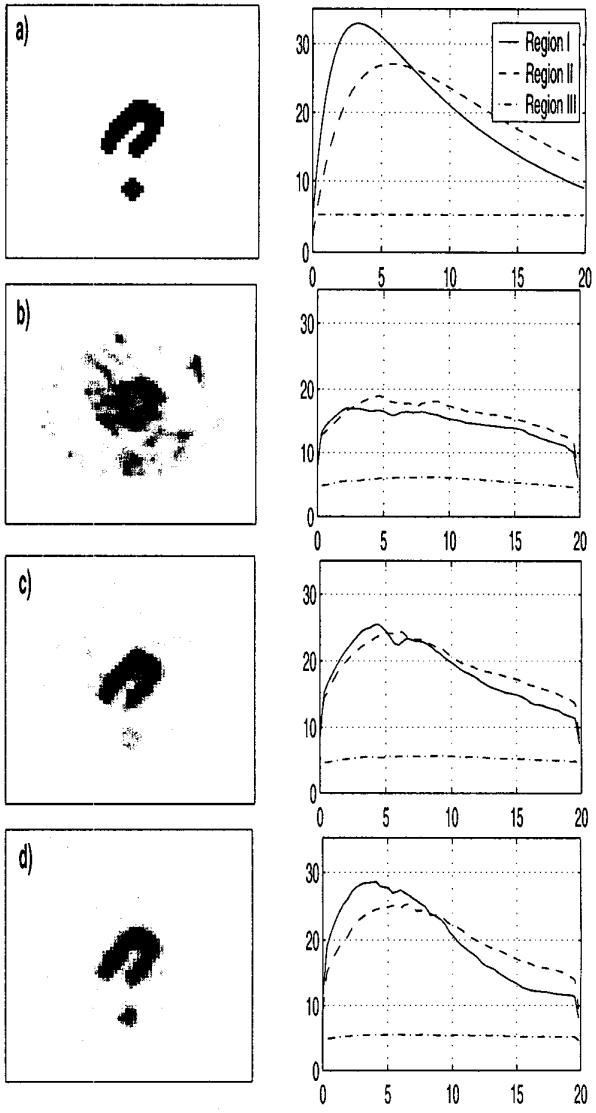

Figure 5: a)The true thorax phantom at t = 5 min, and the time activity curves for each region divided by the number of pixels per region. b) Results of the dSPECT reconstruction are shown for b) single head acquisition, c) dual head camera acquisition, and d) triple head camera acquisition (cf. Table 1).

Acquisition	Region Error		
	I	II	III
Single head	0.58	0.51	1.13
Dual head	0.46	0.47	1.01
Triple head	0.45	0.54	0.94

Table 6a: Weighted errors for dynamic heart simulation.

B. *Phantom and Patient Experiments*

Phantom experiments carried out with a dual head camera (90° configuration) acquired with a rotation of only 90° per head show that the dSPECT method is able to reconstruct both

Region	Peak (min)	A_0 (counts)	$T_{\frac{1}{2},\lambda_1}$ (min)	$T_{\frac{1}{2},\lambda_2}$ (min)
Single head				
I	3.7 ± 2.2	619	0.1	32.7
II	6.1 ± 2.6	1304	0.1	111.5
III	5.9 ± 8.0	8233	0.1	96.8
Dual head				
I	5.5 ± 2.6	1365	0.8	14.3
II	7.1 ± 2.5	2443	0.9	21.0
III	6.2 ± 8.6	7900	0.1	149.0
Triple head				
I	4.6 ± 1.8	1609	0.5	10.2
II	7.3 ± 2.8	2648	0.7	20.1
III	4.0 ± 6.9	7584	0.1	718.9

Table 6b: Parametric fits to dynamic heart simulation (cf. Table 2).

spatial and temporal information quite accurately. Time activity curves for each dynamic region compare very well to the true TA curves (Figure 6). It is recognized that in each case, the dSPECT TA curves are slightly lower in activity compared to the true TA curves, but this can most likely be explained by the fact that the true TA curves are determined from the total number of counts collected by the camera, whereas the dSPECT TA curves only contain counts from a small subset of pixels contained in the 3D ROI. The determination of the peak activity position also appears to perform well, confirming the earlier findings from simulations. In each case, the algorithm is able to find the peak activity position to within a few time points.

Experiment 1

Region	A_0 (counts)	$T_{\frac{1}{2},\lambda_1}$ (min)	$T_{\frac{1}{2},\lambda_2}$ (min)
I	20278	0.04	2.1
II	19467	0.04	3.8
III	17308	0.03	25.8
IV	19493	0.04	6.1
V	18711	0.04	9.3

Experiment 2

Region	A_0 (counts)	$T_{\frac{1}{2},\lambda_1}$ (min)	$T_{\frac{1}{2},\lambda_2}$ (min)
I	19783	0.14	2.1
II	17536	0.19	3.8
III	25088	0.48	5.8

Table 7: Reconstructed parametric values from experimental dynamic data (cf. Table 4).

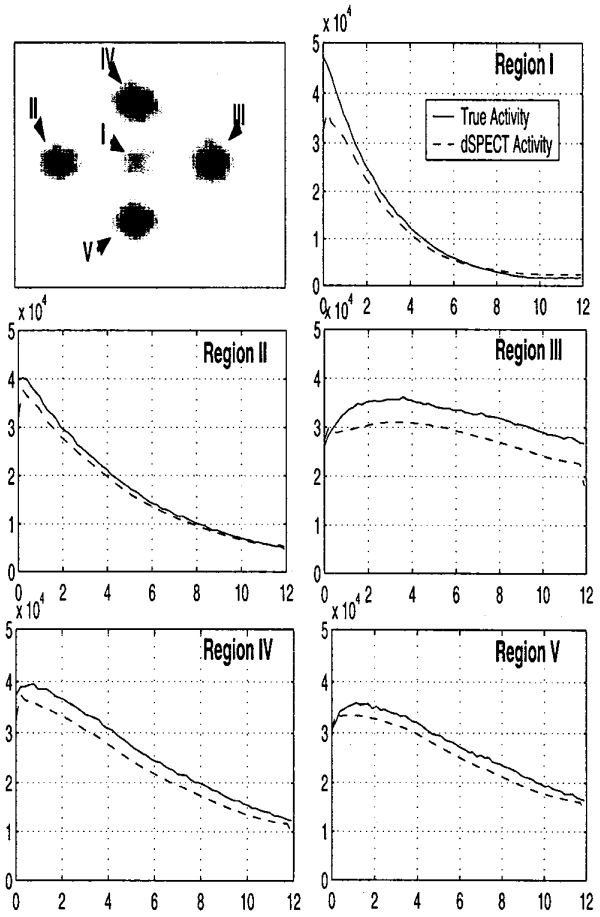

Figure 6: dSPECT reconstruction of dynamic phantom experiment #2 shown at time t=5 min, along with the associated TA curves for each dynamic region. Experiment #1 yielded similar results but are not displayed here.

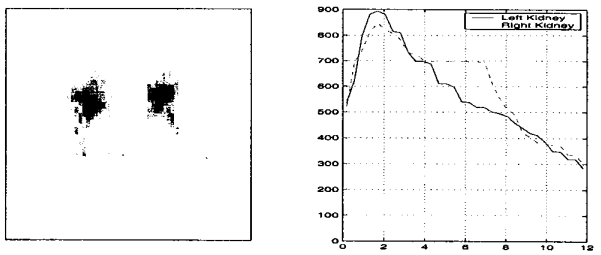

Figure 7: Transaxial image of one dSPECT reconstruction and the TA curve for each renal cortex.

Figure 7 displays a typical transaxial dSPECT reconstruction of a dynamic MAG3 renal scan. The image is shown overlaid on the corresponding attenuation map in order to correlate the images. Shown as well are time activity curves resulting from regions of interest drawn over each renal cortex. It can be seen that in each case, the dSPECT algorithm was able to determine a peak activity position for each pixel. In the case of the time activity curve for the right kidney, it can be seen that a region of no activity change (static activity) is present from t=4 min to t=7 min. This effect is explained in further detail in the Discussion section.

In order to compare the dSPECT result with the planar scan, the dSPECT reconstruction was reprojected into a series of 2D planar images taken at the same angle as seen from the prior planar scan. The result of such a reprojection is shown in Figure 8 along with the TA curves for each renal cortex. It can be seen from these figures, that spatially, the dSPECT reconstruction looks very similar to the planar scan,

but has increased contrast and a higher signal to noise ratio. This is partly due to the higher dose injected for the dSPECT acquisition, but also because depth dependent attenuation correction was done with dSPECT, thus resulting in a higher reconstructed activity. Time activity curves from regions drawn in the dSPECT reprojections are very similar to those obtained over the same region in the planar data set.

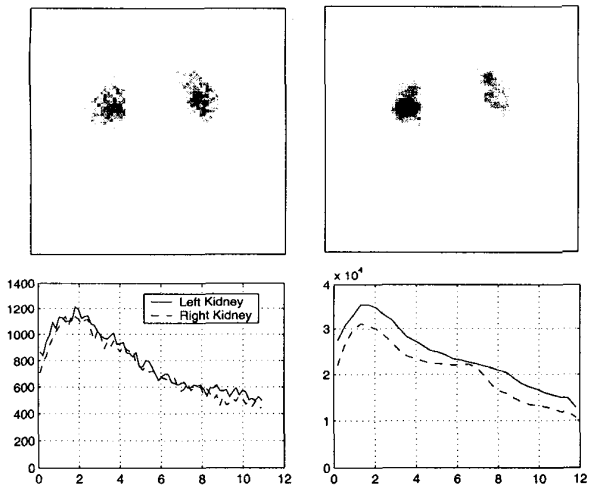

Figure 8: Top: Images of MAG3 renal scan acquired from left) dynamic, planar imaging, and right) reprojection of dSPECT reconstruction into 2D images. Bottom: Time activity curves of renal cortex for both kidneys from left) dynamic, planar images, and right) reprojected dSPECT data.

VI. Discussion

In the case of renal imaging it was seen that in the midst of a decreasing activity, a short time interval was reconstructed as a static distribution. It is postulated that over this time interval, a secondary uptake of activity into this region occured, thus producing an increase in the activity levels for each pixel. Since the CLS algorithm is only able to reconstruct a decreasing or static distribution once the peak has been established, a secondary peak in activity gets reconstructed as a static region.

It is anticipated that in the majority of clinically relevent dynamic imaging applications (myocardial fatty acids, renal imaging, etc), the situation involving multiply peaked pixels will not occur. Rather only a single peak would be present indicating an increase and subsequent decrease in activity over time. While it is possible that a second pass of activity through an organ would produce a second peak of activity, the magnitude of this second peak will usually be of diminished magnitude relative to the first peak due to redistribution throughout the rest of the body.

VII. Conclusion

A modification of the constrained least squares (CLS) method of dynamic SPECT reconstruction has been presented in which the pixel activity is allowed to increase to a certain point in time followed by a decrease thereafter. The time position of this peak activity must be known before the dSPECT reconstruction can occur in order to modify the reconstruction constraints appropriately. A method has been proposed to determine an approximate point of peak activity for each pixel, and to allow flexibility in the selection of this point.

Computer simulations, phantom experiments and patient studies involving slow camera acquisitions of only 180° per head, indicate that the CLS dSPECT algorithm with modified contraints is able to perform accurate dynamic reconstructions with minimal reconstruction artifacts. It has been seen that both two and three head camera geometries outperform single head acquisitions in all circumstances by a wide margin. However, the difference between dual and triple head acquisitions is almost negligible in most clinically relevant situations (ie, presence of Poisson noise, inhomogeneous attenuation). In fact, in a preliminary dynamic renal study, an acquisition involving a dual head camera and only a 90° rotation was able to provide results comparable to planar, dynamic imaging.

VIII. References

[1] K. Nakajima, J. Taki, H. Bunko, M. Matsudaira, A. Muramori, I. Matsunari, K. Hisada, and T. Ichihara, "Dynamic acquisition with a three-headed SPECT system: application to technetium 99m-SQ30217 myocardial imaging," *J. Nuc. Med.*, vol. 32, pp. 1273–1277, 1991.

[2] A. Smith, G. Gullberg, P. Christian, and F. Datz, "Kinetic modeling of teboroxime using dynamic SPECT imaging of a canine model," *J. Nuc. Med.*, vol. 35, pp. 484–495, 1994.

[3] T. Farncombe, A. Celler, D. Noll, J. Maeght, and R. Harrop, "Dynamic SPECT imaging using a single camera rotation (dSPECT)," *IEEE Trans. Nuc. Sci.*, vol. 46, no. 4, pp. 1055–1061, 1999.

[4] J. Maeght, D. Noll, A. Celler, and T. Farncombe, "Methods for dynamic SPECT." Laboratoire MIP Technical Report, 1999. http://mip.ups-tlse.fr/publi/rapp99/99.26.html.

[5] M. Hudon, D. Lyster, W. Jamieson, A. Qayumi, M. Keiss, L. Rosado, A. Autor, C. Sartori, H. Dougan, and J. V. D. Broek, "Efficacy of (^{123}I)-iodophenyl pentadecanoic acid (IPPA) in assessment myocardial metabolism in a model of reversible global ischemia," *Eur. J. Nuc. Med.*, vol. 14, pp. 594–599, 1988.

[6] A. Celler, T. Farncombe, R. Harrop, and D. Lyster, "Dynamic heart-in-thorax phantom for functional SPECT," *IEEE Trans. Nuc. Sci.*, vol. 44, no. 4, pp. 1600–1605, 1997.